Microscopic charging and in-gap states in superconducting granular aluminum

Fang Yang,[1,2] Thomas Gozlinski,[2] Tim Storbeck,[2] Lukas Grünhaupt,[2] Ioan M. Pop,[2,3] and Wulf Wulfhekel[2,3]
[1]*Institute for Nanoelectronic Devices and Quantum Computing, Fudan University, 200438 Shanghai, China*
[2]*Physikalisches Institut, Karlsruhe Institute of Technology, 76131 Karlsruhe, Germany*
[3]*Institute of Quantum Materials and Technologies, Karlsruhe Institute of Technology, 76344 Eggenstein-Leopoldshafen, Germany*

(Received 30 January 2020; revised 17 August 2020; accepted 19 August 2020; published 8 September 2020)

We present scanning tunneling microscope (STM) measurements of the local electronic structure of superconducting granular aluminium films. The STM spectra show a homogeneously increased superconducting gap compared to that of aluminum, both near and above the Mott resistivity $\rho_M \approx 400 \mu\Omega\,\mathrm{cm}$. Above ρ_M we find Coulomb charging effects, a first indication of electrical decoupling, and in-gap states on individual grains, which could contribute to flux noise and dielectric loss in quantum devices. We also observe multiple low-energy states outside the gap, which indicate bosonic excitations of an energy below twice the superconducting gap.

DOI: 10.1103/PhysRevB.102.104502

I. INTRODUCTION

Superconducting granular metals are interesting model systems, because their microstructure can be seen as a network of artificial atoms coupled by electron tunneling, giving rise to rich physical phenomena [1,2]. They display a complex phase diagram [3–5], with a superconductor-to-insulator transition (SIT) and a nonmonotonic dependence of the critical temperature vs resistivity [2,4]. Whether the SIT is driven by disorder [6–10] or charging effects [11–15] remains an open question. Beyond fundamental relevance, these mechanisms also govern noise and dissipation in microwave circuits [16,17].

Granular aluminum (grAl) is a particularly appealing material due to its ease of fabrication and compatibility with standard Al/AlO$_x$/Al Josephson junction technology. Tuning the oxygen partial pressure during aluminum deposition results in a granular structure of crystalline Al grains in an amorphous AlO$_x$ matrix as has been observed by transmission electron microscopy [3], film resistivities ρ from 10 to $10^5\ \mu\Omega\,\mathrm{cm}$, and consequently variable intergrain coupling. As a function of ρ, the critical temperature T_c of grAl increases compared to pure aluminum [1,3], reaching a maximum in the vicinity of the Mott resistivity $\rho_M \approx 400\,\mu\Omega\,\mathrm{cm}$ [12,18], after which it decreases, and the system becomes insulating at $\rho \approx 10\,\mathrm{m}\Omega\,\mathrm{cm}$. Thanks to its large kinetic inductance [19], low microwave frequency losses [20–23] and amenable nonlinearity [24,25], grAl is also a valuable material for quantum engineering.

Although grAl has been successfully employed in fluxonium quantum bits [26,27], alongside other high impedance materials such as NbTiN [28], the realization of superconducting quantum processors requires orders of magnitude improvement in coherence. This task is complicated by the fact that several types of imperfections, both microscopic and macroscopic, are concomitantly present, depending on system design, microfabrication technology, and materials [29]. So far, microscopic defects have been measured rather indirectly, through their interaction with the device itself [30,31]. It is therefore clear that a local probe, such as scanning tunneling microscopy (STM), can offer precious complementary information about the nature of the observed defects, be that localized spins, charge states, or other microscopic systems, and can contribute to a microscopic understanding of the phase diagram of superconducting granular metals in general. Here, we employ the imaging abilities of a 30 mK STM, capable of high energy-resolution spectroscopy [32], to resolve localized charge states and to test the presence of low energy excitations both inside and outside the superconducting gap of grAl.

II. EXPERIMENTAL RESULTS

A. Film preparation and measurement setup

The measurement geometry of the experiment is sketched in Fig. 1(a). The samples consist of 50 nm thick grAl films deposited by electron beam evaporation of pure Al at a rate of $1\,\mathrm{nm\,s}^{-1}$ in an oxygen atmosphere of partial pressures of 2.8×10^{-5} mbar for oxygen poor samples of $\rho \approx 300\,\mu\Omega\,\mathrm{cm}$, and 5.6×10^{-5} mbar for oxygen rich samples of $\rho \approx 2 \times 10^3\ \mu\Omega\,\mathrm{cm}$, following established growth recipes [3,26]. The corresponding superconducting critical temperature is approximately 2 K (see Appendix). During deposition the substrate was at room temperature, and we used the same setup as in our recent study of the SIT of grAl, allowing a direct comparison [5]. For these types of films, the SIT is observed for a room temperature resistivity $\rho \approx 10\,\mathrm{m}\Omega\,\mathrm{cm}$.

We used Nb doped (0.7 weight %) SrTiO$_3$ (Nb:STO) single crystals as substrates, in order to start with a conducting, flat, and nonreactive surface. The substrate is expected to become superconducting at temperatures below 200 mK [33]. Since the thickness of the grAl films is much larger than the grain size of 3 to 5 nm [3], the films show a bulklike behavior,

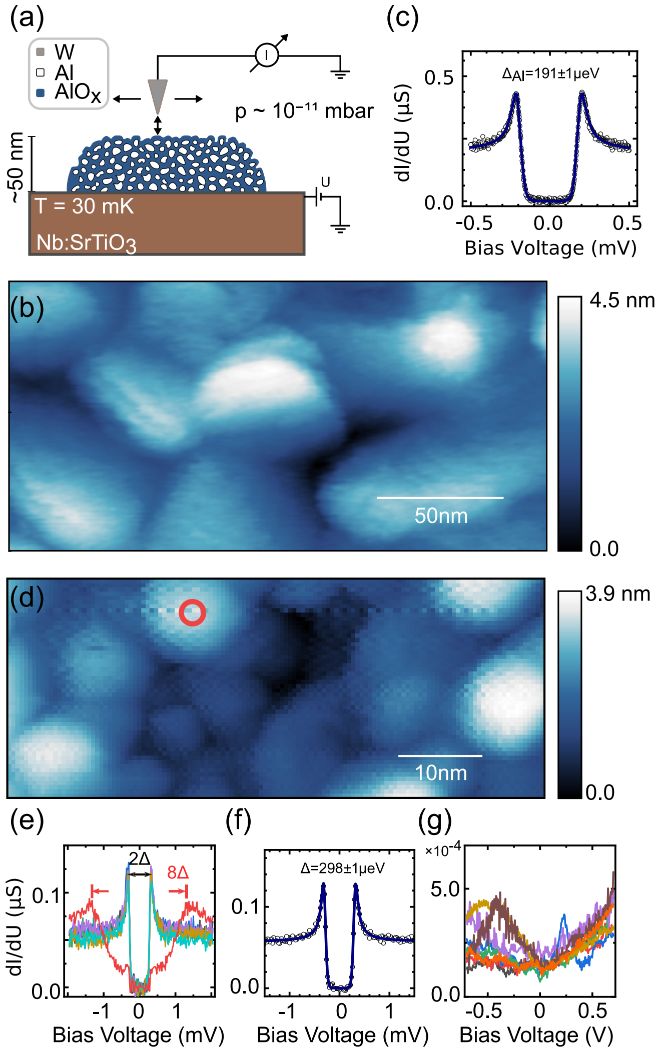

FIG. 1. (a) Schematic drawing of the experimental configuration. (b) STM image of a pure Al film ($U = -1$ V, $I = 100$ pA). (c) dI/dU of the pure Al film with a superconducting gap Δ close to that of bulk Al ($U = 1$ mV, $I = 100$ pA, $\Delta U_{\mathrm{rms}} = 1.4\,\mu$V). (d) STM image of an oxygen poor grAl film ($\rho \approx 300\,\mu\Omega$ cm, $U = 60$ mV, $I = 240$ pA). (e) dI/dU recorded on different grains. All measured grains show the same gap $\Delta = 291\,\mu$eV ($U = 2$ mV, $I = 107$ pA, $\Delta U_{\mathrm{rms}} = 15\,\mu$V). The red curve was recorded on the grain marked with a red circle in (d). (f) Averaged spectrum (open circles) of (e), excluding the red curve, and BCS fit (blue line) including instrumental broadening. (g) Large bias range dI/dU measured on different grains, showing essentially a metallic behavior ($T = 1$ K, $U = 700$ mV, $I = 156$ pA, $\Delta U_{\mathrm{rms}} = 3$ mV).

i.e., most of the grains reside inside the film and determine the transport properties. It is therefore not surprising that the measured properties of grAl films are consistent between various substrates, such as glass, silicon or sapphire [3,5]. For test purposes, deposition was also carried out in parallel on an insulating substrate placed next to the Nb:STO sample to verify the film resistivity by transport experiments.

Immediately after deposition, in order to avoid surface oxidation of the grAl films, the samples were transferred to the ultra high vacuum of the STM system using a vacuum suitcase. STM measurements were carried out at a base temperature of 30 mK (deviating temperatures are indicated in the figure captions). For topographic images, the bias voltage U is selected to be much above the superconducting gap Δ and the STM is operated in the constant current mode at fixed working point of a sample bias U and a tunneling current I. To obtain information on Δ, the feed-back loop is opened, the position of the tip is fixed, and U is ramped, while the differential conductivity dI/dU is measured.

B. Pure Al films

As a control experiment, we measured a 30 nm thick pure Al film, i.e., without oxygen exposure during growth. Figure 1(b) shows an STM image of the film consisting of crystallites of about 50 nm lateral size. The large size of the crystallites is due to the high diffusion mobility of Al, according to its relatively low melting point compared to AlO_x. Figure 1(c) shows the the coherence peaks and a superconducting gap Δ_{Al} of 191 μeV obtained by a fit to the BCS density of states (DOS). This is close to the known values [34] for thin-film Al (42 nm thick) of 200 μeV. In all respects, the pure Al sample behaves as expected.

C. Oxygen poor samples

In contrast, Fig. 1(d) shows a topographic image of a grAl film with $\rho \approx 300\,\mu\Omega$ cm, i.e., close to ρ_{M} and the maximum $T_C = 2.1$ K of the superconducting dome [5]. Superconducting grAl can be viewed as a connected 3D network of Al grains, separated by amorphous AlO_x. As evident from Fig. 1(d), the Al grains in grAl are much smaller compared to the pure Al film, as expected [3]. Note that the STM tip, etched from a W wire, cannot be made to arbitrary sharpness. Since the topographic image reflects a convolution of the grains and the tip shape, the grains may appear slightly larger in STM images. The observed distribution of grain sizes, 5 to 10 nm, agrees with the reported values and spread in the literature for similar film growth conditions [3].

Figure 1(e) shows a selection of dI/dU spectra recorded on different grains. They show a practically identical superconducting gap $\Delta = 298\,\mu$eV, obtained with a BCS fit [see Fig. 1(f)]. Note that this value is significantly larger than that of pure Al. For similar grAl films, radio-frequency measurements [21] revealed a bulk value for Δ of approximately 344 μeV, extracted from the measurement of the critical temperature T_C, while direct THz spectroscopy [5] revealed a value of $336 \pm 8\,\mu$eV. Taking into account the lower surface oxidation of the ultrahigh vacuum samples, the surprisingly small difference between these values, obtained using very different methodologies, indicates that grains residing at the surface have a superconducting gap comparable to the bulk of the grAl sample. Additionally, from the fact that all measured grains show the same Δ, we conclude that either the gap enhancement mechanism is homogeneous and robust to variations in grain size, or the grains are coupled strongly enough to even out Δ variations.

On a larger energy scale [see Fig. 1(g)] the grains show a metallic behavior, i.e., a DOS that has no conventional band gap. However, the dI/dU spectra are quantitatively different

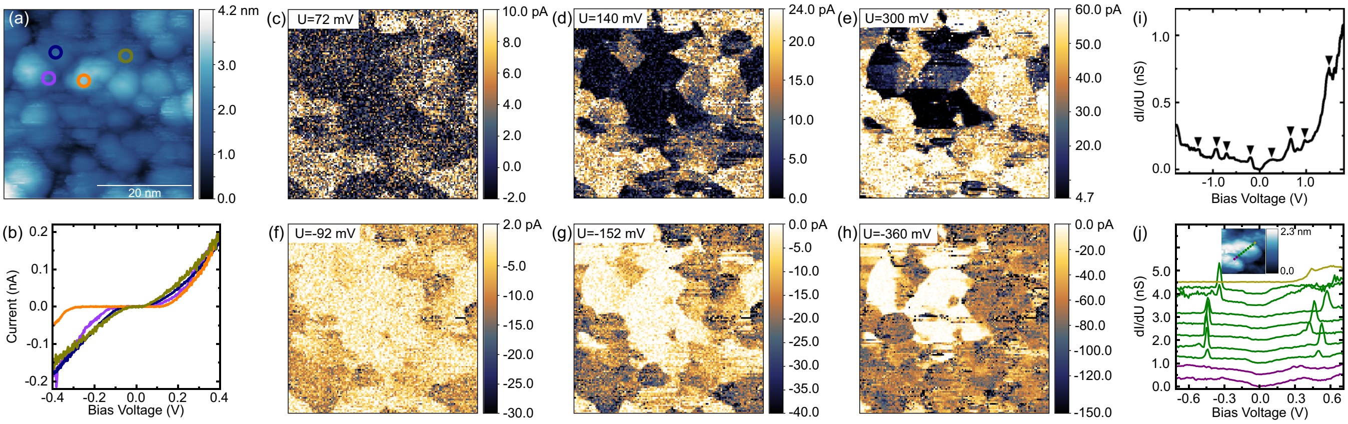

FIG. 2. (a) STM image of the oxygen rich grAl film ($\rho \approx 2 \times 10^3\ \mu\Omega\,\mathrm{cm}$, $U = 400$ mV, $I = 180$ pA). (b) Averaged $I(U)$ spectra of grains marked by the colored circles in (a) with same feedback parameters. (c)–(h) Maps of the local tunneling current I for the same area as in (a) at positive, (c)–(e), and negative, (f)–(h), bias voltages, as indicated by the labels (tip stabilized at: $U = 400$ mV, $I = 180$ pA). (i) Typical dI/dU spectrum of an individual grain at energies much higher than Δ showing charging peaks, marked by triangles ($U = 1.8$ V, $I = 550$ pA, $U_{\mathrm{rms}} = 21$ mV). (j) Series of dI/dU spectra recorded on a line crossing three grains (c.f. topographic inset—$20 \times 20\ \mathrm{nm}^2$) indicated by purple, green, and yellow (neighboring curves are shifted by 0.5 nS, $U = 700$ mV, $I = 200$ pA, $\Delta U_{\mathrm{rms}} = 7$ mV).

from grain to grain. The fact that we do not observe a common DOS over several grains indicates that the electron wave functions are not entirely delocalized, and electrons do not move in a ballistic way, which is expected considering the contact between randomly oriented granular Al crystallites.

Note that occasionally individual grains show a deviating behavior, as indicated by the red circle in Fig. 1(d) and the corresponding red dI/dU spectrum in Fig. 1(e). The low energy spectrum of the grain shows reduced coherence peaks due to the feedback parameters set at 2 mV and a secondary gap of approximately 8Δ. These are the first indications of what will be observed in grAl films with a higher oxygen concentration.

Note that the features of the dI/dU spectra do not change with feed-back parameters in a wide range, i.e., the results do not depend on the tips-sample distance as illustrated in the Appendix. In all spectra recorded on oxygen poor samples, the superconducting gap was fully developed. We did not observe any in-gap states. When, however, extreme tunneling conditions of high tunneling conductivity were chosen, also cotunneling effects, i.e., Andreev reflections or Cooper pair tunneling, become visible (see Appendix). For the results presented here we operated below the cotunneling regime.

D. Oxygen rich samples

In Fig. 2 we summarize the behavior of grains in oxygen rich films ($\rho \approx 2 \times 10^3\ \mu\Omega\,\mathrm{cm}$). In topography [see Fig. 2(a)] we observe grains of similar size compared to the oxygen poor films, in agreement with previous results [3]. From the large range $I(U)$ measurements shown in Fig. 2(b), taken on the individual grains highlighted in Fig. 2(a), it becomes obvious that the grains do not entirely behave metallic but only show large currents above a certain threshold voltage in the range of roughly 70 to 300 meV. The $I(U)$ curves also vary from grain to grain. In Figs. 2(c)–2(e), we plot measured maps of the tunnel current at several bias voltages. Multiple neighboring grains show a sudden increase in current, indicating that they form stronger electrically coupled clusters or electrical islands. We measure the same behavior for negative polarity of the bias voltage [see Figs. 2(f)–2(h)]. Moreover, charging effects are also apparent in dI/dU in Fig. 2(i). Resonant tunneling causing peaks in dI/dU, marked by black triangles, can be seen. Such series of peaks are commonly observed in the Coulomb blockade regime at voltages when the chemical potential of the lead hits the second, third, etc. charging states of the island [35]. The charging energies of ±70 to ± 300 meV correspond to capacities between 0.3 and 1.1 aF. Approximating the electrical islands by a simple sphere, the corresponding diameters range from 5 to 20 nm in qualitative agreement with our topographic STM measurements.

We also observe charging localized on a single grain. In Fig. 2(j) we show a series of dI/dU curves recorded on a line extending over three grains. Measurements on each grain are indicated by purple, green, and yellow spectra. The features of the spectra are qualitatively similar when the STM tip probes the same grain, however, in between the grains, the spectra change discontinuously.

Since STM is only sensitive to the surface, one can speculate that grains inside the film are coupled to more neighbors, exhibiting less charging. However, for films with thickness comparable to the grain size, charging effects could be dominant. Indeed, recent measurements of a grAl transmon quantum bit, employing a 10 nm thick film, also suggest that grains couple in clusters [25], comparable to the ones visible in Figs. 2(c)–2(h).

From the measured low energy spectrum in Fig. 3, we confirm that the grains are superconducting, with a similarly enhanced superconducting gap Δ. The current density used for the measurement of the low-energy tunneling spectra is three orders of magnitude below the bulk critical current density of similar films [36], so we expect the measurement to be nondisruptive. Interestingly, for oxygen rich films we observe a series of peaks outside Δ. We can only speculate on

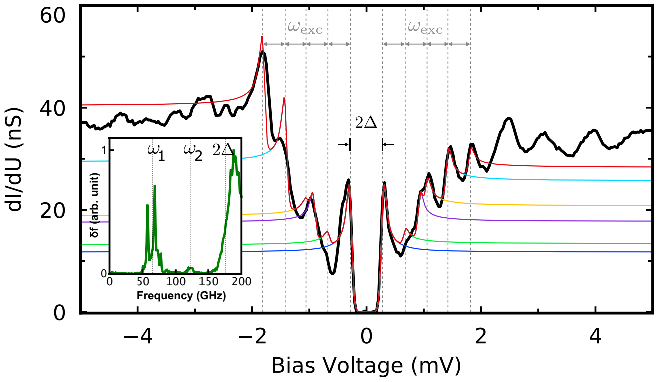

FIG. 3. The black line shows a typical high resolution dI/dU spectrum of a grain, which displays a superconducting gap and several sharp peaks (excitations) outside the gap ($U = 7$ mV, $I = 270$ pA, $\Delta U_{\rm rms} = 14\,\mu$V). The red line shows a fit to a model of five energetically symmetric inelastic excitations also indicated individually in other colors. Excitation energies of multiples of $\omega_{\rm exc}$ and the gap Δ are indicated by dashed lines. The inset reproduces THz spectroscopy measurements of samples with $\rho \approx 2 \times 10^3\,\mu\Omega\,$cm from Ref. [5].

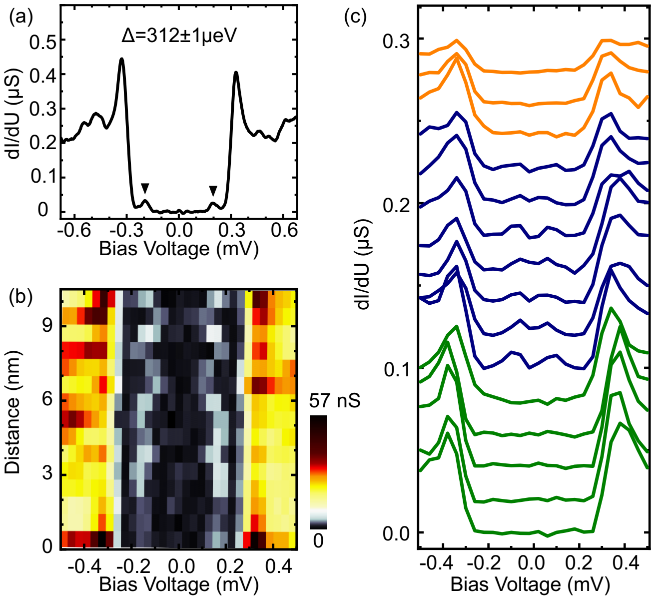

FIG. 4. (a) dI/dU spectrum showing two in-gap states, highlighted by triangular markers, at $\pm 200\,\mu$V ($\rho \approx 2 \times 10^3\,\mu\Omega\,$cm, $U = 0.7$ mV, $I = 10$ pA, energy resolution $20\,\mu$V). (b) Color coded dI/dV as a function of lateral tip position, recorded on a straight line, across one grain. The in-gap states shift symmetrically in energy with respect to the origin as a function of tip position ($U = 4$ mV, $I = 100$ pA, $\Delta U_{\rm rms} = 20\,\mu$V). (c) A series of dI/dU spectra recorded in a straight 18 nm line crossing three grains indicated by green, blue, and orange. The two outer grains do not show in-gap states, while the inner grain displays in-gap states at $\approx \pm 100\,\mu$V ($U = 4$ mV, $I = 100$ pA, $\Delta U_{\rm rms} = 25\,\mu$V).

the origin of this presumably many body effect. The energy and sharpness of the peaks are distinctly different from the charging effects shown in Figs. 2(i) and 2(j) and resemble in sharpness the coherence peaks. This might indicate inelastic tunneling, i.e., the energy of the initially tunneling electron is shared between an excited boson of defined energy, and the scattered electron ending up in the peaked BCS single particle DOS of the superconductor. This would show up in the dI/dU spectra as copies of the peaked BCS DOS shifted in energy away from zero bias by the boson energy. Each excited state contributes one peak and one steplike increase in dI/dU, as indicated by the colored traces in Fig. 3.

We can rule out phonons in this case, as neither the small energetic shifts in the low meV range correspond to the energies of the van Hove singularities of the phonon DOS of Al or AlO$_x$ (all above 15 meV), nor are they observed on pure or low oxygen Al films. Possible bosonic excitations are Higgs modes in the granular superconductor [37,38] or two-dimensional plasma phase modes [5], i.e., excitations of the size or phase of the superconducting order parameter. The sharpness of the peaks does not agree with simple pair breaking by inelastic tunneling, in which the electrons would quickly recombine making theses excitations strongly damped and invisible as in ordinary superconductors. Also the peaks appear as a series corresponding to an excitation ladder with a boson energy lower than 2Δ (a hot tunneling electron can excite zero, one, two, etc. bosons.). In Ref. [5], for oxygen rich samples prepared in the same deposition setup, two-dimensional plasma phase modes in THz spectroscopy of an energy $\omega_1 < \Delta$ and an unidentified second excitation at $\omega_2 \approx 1.4\Delta$ were observed, which could be responsible for the peaks in the oxygen rich films (see inset of Fig. 3). In other granular superconductors near the SIT, Higgs modes were reported [37,38] with long lifetimes and an energy slightly below 2Δ down to very low energies depending on the disorder. Our spectroscopic data only reveals the energy of the states but not their origin.

In order to analyze the spectrum, we fitted the inner gap and quasiparticle peaks with a simple BCS fit of the DOS for elastic tunneling (dark blue line in Fig. 3). To model inelastic excitations, we shifted and scaled in intensity the single particle spectrum by the inelastic excitation energy ω for positive and negative bias and added the inelastic conductivity to the elastic one as indicated by the colored lines. Lifetime broadening of the excitations were neglected and five excitations were taken into account. As can be seen, this fit (red line) qualitatively reproduces the complex spectrum with excitations that are regular and symmetric with respect to their energy but not their intensity. We note that the energies of four of the observed peaks (or shoulders) are multiples of $\omega_{exc} = \omega_2 \approx 1.4\Delta$ that we found also in the THz absorption experiments on films of similar sheet resistance (see inset Fig. 3). We can thus state that both experiments show an excitation at ω_2. The nature of these excitations needs to be further explored, both theoretically and experimentally. One excitation (plotted in purple) in the observed spectrum, however, does not fall on an integer multiple of this mode.

We now focus on the superconducting gap in oxygen rich samples. Figure 4(a) shows a high resolution spectrum of the superconducting gap with $\Delta = 312 \pm 1\,\mu$V obtained from a BCS fit. The gap Δ measured on different grains is slightly higher compared to the oxygen poor samples [cf. Fig. 1(f)].

However, about half of the grains (11 out of 23) show in-gap states, as indicated by triangles in the dI/dU spectrum of Fig. 4(a). These states are of rather low intensity, but their energetic position rules out Andreev reflections of the tip electrons as their origin. Instead, the observation of the Kondo effect in grAl films above T_C [39] suggests that unpaired electrons or magnetic moments give rise to Yu-Shiba-Rusinov (YSR) in-gap states. The energy of YSR states is a continuous function of the exchange coupling to the superconductor [40] and of the charging energy of the grain or cluster of grains.

Similarly to Ref. [13], we consider two scenarios for the origin of the unpaired spins. First, the finite size of the grains and the fact that some are only weakly coupled to the rest of the grAl film might result in an odd number of charges on individual grains in equilibrium, as suggested by Deutscher *et al.* [39]. The interaction of these unpaired electrons with the superconducting condensate may induce YSR states. Second, the nonstoichiometric composition of the AlO_x in between the pure Al grains may lead to unpaired electrons trapped in the insulating barriers. The interaction of these localized moments with the superconductor could give rise to YSR states.

In order to discriminate between the above scenarios, we measured the spacial dependence of the YSR states on a line crossing a single grain. While the superconducting gap Δ remains constant, as shown in Fig. 4(b), the in-gap states vary in energy as a function of the STM tip position. In the scenario of electrically decoupled grains with an odd number of electrons, the electric field of the STM tip would change the chemical potential of the grain, the coherence peaks would shift with tip position, but the energy of the YSR states with respect to the gap edge would be fixed. This is in contrast with our observations.

If however the unpaired spins reside in the oxide, the electric field of the tip can change their energy, and consequently the exchange coupling to the grain, as in the study of Farinacci *et al.* [40]. In this case the YSR state shifts with tip position, while the coherence peaks remain unaffected. This scenario agrees with our measurements. Moreover, Fig. 4(c) illustrates the strong localization of the YSR states on particular grains: Only the middle grain (blue spectra) shows in-gap states at $\pm 100\,\mu$eV.

III. DISCUSSION

In summary, using STM spectroscopy we have observed an enhanced and homogeneous superconducting gap for both oxygen poor and rich grAl samples. In the oxygen rich samples the grains start to decouple, charging effects set in, and when fully developed eventually leading to the SIT. Hand in hand with this decoupling, we observed a secondary gap and excitations with an energy comparable to the superconducting gap, as well as YSR states in some of the grains, possibly related to unpaired electrons in the oxide barriers. For the YSR states to exist, the localized spins in the oxide need to exchange couple with the superconducting grain. If the oxide is sufficiently thin, the states in the oxide delocalize in the electron gas of the film and we cannot think in terms of localized impurity spins anymore. Thus, in the fully metallic oxygen poor samples, we do not observe in-gap states. When the oxide becomes thicker the unpaired spin in the oxide couple less to the grains and localize. This interpretation is consistent with the fact that the YSR states appear only when also the grains start to decouple, i.e., for resistivities larger than ρ_M. This further suggests that in order to minimize the local sources of quantum decoherence in devices containing Josephson junctions it is advantageous to use very thin oxide films for the insulating barrier to prevent the localization of unpaired electrons in the barrier.

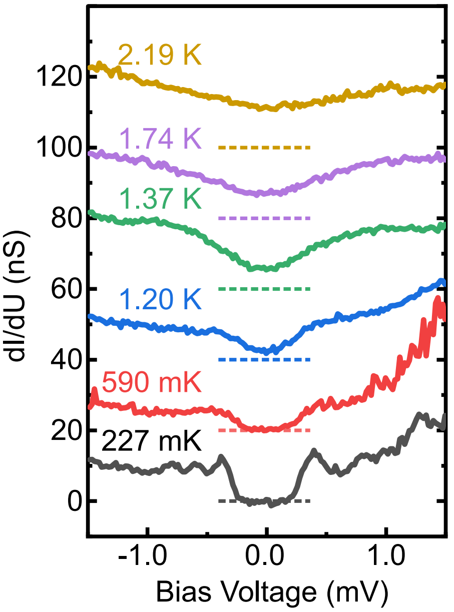

FIG. 5. dI/dU spectra for the oxygen-rich sample measured at temperatures as indicated. The tunneling conductance was recorded when the sample was warming up. The offset of each spectrum is indicated by dashed lines in corresponding colors. The feedback condition was set to be $U = 2$ mV, $I = 30$ pA, $U_{\mathrm{rms}} = 70\,\mu$V.

The existence of in-gap YSR states can be detrimental for grAl quantum devices in several ways: They can introduce additional dissipation in the microwave domain, as they are located inside the gap, or even alter the spectrum of the devices in the form of discrete states, if they couple sufficiently strong [30]. The presence of spins with their magnetic moment may also contribute to the flux noise observed in grAl devices [26]. As most pure Al devices are exposed to the ambient during microfabrication, these spins can form in the natural oxide at the surface and similarly in the Josephson junction barrier. A deeper understanding of the formation of localized spins in the oxide by measuring the density of YSR states versus resistivity in grAl, and also in native Al oxide, with the goal of reducing their impact on coherence in quantum devices has the potential to enhance coherence times in these devices.

ACKNOWLEDGMENTS

W.W. acknowledges funding by the Deutsche Forschungsgemeinschaft (DFG) under Grant No. WU 349/12-1. I.M.P and L.G. acknowledge the Alexander von Humboldt Foundation in the framework of a Sofja Kovalevskaja award endowed by the German Federal Ministry of Education and Research. F.Y. acknowledges funding from the Alexander von Humboldt foundation in the framework of Humboldt Research Fellowship for Postdoctoral Researchers.

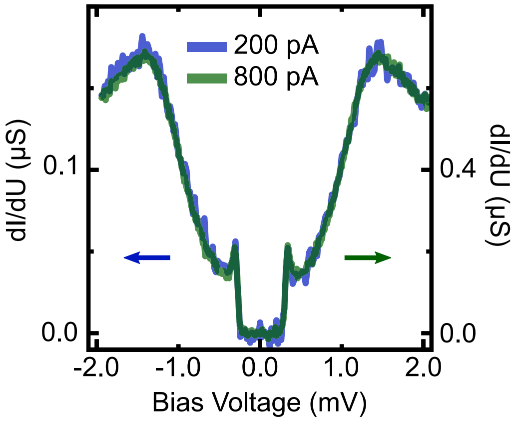

FIG. 6. dI/dU spectra recorded with different tunneling conductance on a relatively insulated grain of the oxygen-poor sample. On the grain marked by the red circle in Fig. 1(d), dI/dU with different tunneling conductance were measured. The feedback condition for the blue curve was set to be $U = 2$ mV, $I = 200$ pA, and for the green curve $U = 2$ mV, $I = 800$ pA. For both, $U_{\mathrm{rms}} = 21\ \mu$V.

APPENDIX

We measured the superconducting gap of the oxygen-rich sample at different temperatures. As shown in Fig. 5, the superconducting gap smears out with increasing temperature and eventually vanishes. From the limited number of measurements at various temperatures, we find that the superconducting transition occurs between 1.74 K and 2.19 K.

In STM experiments the signal current flows through the tip-sample junction. In our measurements, the size and position of the reported features do not depend on the tunneling conductance, as illustrated in Fig. 6. The two dI/dU curves in Fig. 6 were measured on the more insulated grain marked by a red circle in Fig. 1(d). The shape of the curves is identical, despite the factor four change in the tunneling conductance, i.e., only sample properties enter the dI/dU curves, and there are no detectable voltage drops inside the granular film. We conclude that the tunneling resistance of the tip-sample junction dominates over other resistors in series in the electronic circuit.

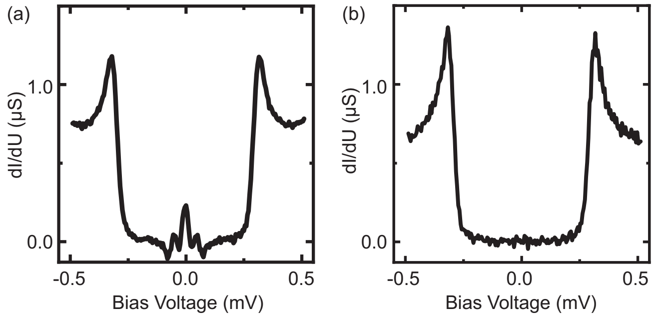

FIG. 7. (a) dI/dU spectrum recorded on the relatively insulated grain of Fig. 6. (b) dI/dU spectrum recorded on a normal metallic grain of the oxygen-poor sample. Feedback condition: $U = 500\ \mu$V, $I = 200$ pA, $U_{\mathrm{rms}} = 14\ \mu$V.

By further increasing the tunneling conductance to the scale of μS approaching the critical current, features of Andreev reflections or Josephson tunneling start to appear in the dI/dU spectrum as a sharp peak at zero bias surrounded by in-gap oscillations including negative differential conduction [41–43] as shown in Fig. 7(a) recorded on the same grain as in Fig. 6. Thus, the spectrum does not anymore represent the DOS of the sample but also contains information about cotunneling events (tunneling of two quasiparticles or a Cooper pair). Zero bias peaks have been reported at large currents in transport between two superconductors, i.e., in our case the grains inside the film. Here, this transport channel between grains is in series with the tunneling junction between the tip and the sample. When the currents are high enough that a small voltage drop arises in the transport inside grAl these cotunneling processes of two electrons are expected. They only become visible at high currents [41,42]. When moving the tip from the more insulated grain to another grain that did not show any indication of insulation, the zero bias peak vanishes accordingly even at the severe tunneling condition [see Fig. 7(b)]. The Andreev reflection with the peak at zero bias voltages is in sharp contrast to YSR states shown in Fig. 3, which appear as symmetric peaks in the otherwise fully gapped spectrum [40]. The energetic position of the YSR states is variable and depends on the exchange coupling of the unpaired spin to the superconductor [40]. In our case, the energies of the YSR states varied between 150 and 225 μV. This also distinguishes them from Andreev reflections at zero bias and Andreev bound states that display an energy of fixed ratio to the superconducting gap Δ [41].

---

[1] R. W. Cohen and B. Abeles, Phys. Rev. **168**, 444 (1968).

[2] I. S. Beloborodov, A. V. Lopatin, V. M. Vinokur, and K. B. Efetov, Rev. Mod. Phys. **79**, 469 (2007).

[3] G. Deutscher, H. Fenichel, M. Gershenson, E. Grünbaum, and Z. Ovadyahu, J. Low Temp. Phys. **10**, 231 (1973).

[4] U. S. Pracht, N. Bachar, L. Benfatto, G. Deutscher, E. Farber, M. Dressel, and M. Scheffler, Phys. Rev. B **93**, 100503(R) (2016).

[5] F. Levy-Bertrand, T. Klein, T. Grenet, O. Dupré, A. Benoît, A. Bideaud, O. Bourrion, M. Calvo, A. Catalano, A. Gomez, J. Goupy, L. Grünhaupt, U. v. Luepke, N. Maleeva, F. Valenti, I. M. Pop, and A. Monfardini, Phys. Rev. B **99**, 094506 (2019).

[6] P. W. Anderson, Phys. Rev. **109**, 1492 (1958).

[7] B. Sacépé, C. Chapelier, T. I. Baturina, V. M. Vinokur, M. R. Baklanov, and M. Sanquer, Phys. Rev. Lett. **101**, 157006 (2008).

[8] B. Sacepe, T. Dubouchet, C. Chapelier, M. Sanquer, M. Ovadia, D. Shahar, M. Feigel'man, and L. Ioffe, Nat. Phys. **7**, 239 (2011).

[9] E. F. C. Driessen, P. C. J. J. Coumou, R. R. Tromp, P. J. de Visser, and T. M. Klapwijk, Phys. Rev. Lett. **109**, 107003 (2012).

[10] M. Mondal, A. Kamlapure, M. Chand, G. Saraswat, S. Kumar, J. Jesudasan, L. Benfatto, V. Tripathi, and P. Raychaudhuri, Phys. Rev. Lett. **106**, 047001 (2011).

[11] N. F. Mott, Rev. Mod. Phys. **40**, 677 (1968).

[12] R. C. Dynes, J. P. Garno, G. B. Hertel, and T. P. Orlando, Phys. Rev. Lett. **53**, 2437 (1984).

[13] N. Bachar, S. Lerer, S. Hacohen-Gourgy, B. Almog, and G. Deutscher, Phys. Rev. B **87**, 214512 (2013).

[14] N. Bachar, S. Lerer, A. Levy, S. Hacohen-Gourgy, B. Almog, H. Saadaoui, Z. Salman, E. Morenzoni, and G. Deutscher, Phys. Rev. B **91**, 041123(R) (2015).

[15] A. G. Moshe, E. Farber, and G. Deutscher, Phys. Rev. B **99**, 224503 (2019).

[16] M. V. Feigel'man and L. B. Ioffe, Phys. Rev. Lett. **120**, 037004 (2018).

[17] R. Kuzmin, R. Mencia, N. Grabon, N. Mehta, Y.-H. Lin, and V. E. Manucharyan, Nat. Phys. **15**, 930 (2019).

[18] R. C. Dynes and J. P. Garno, Phys. Rev. Lett. **46**, 137 (1981).

[19] H. Rotzinger, S. T. Skacel, M. Pfirrmann, J. N. Voss, J. Műnzberg, S. Probst, P. Bushev, M. P. Weides, A. V. Ustinov, and J. E. Mooij, Superconductor Science and Technology **30**, 025002 (2016).

[20] L. Grünhaupt, N. Maleeva, S. T. Skacel, M. Calvo, F. Levy-Bertrand, A. V. Ustinov, H. Rotzinger, A. Monfardini, G. Catelani, and I. M. Pop, Phys. Rev. Lett. **121**, 117001 (2018).

[21] F. Valenti, F. Henriques, G. Catelani, N. Maleeva, L. Grünhaupt, U. von Lüpke, S. T. Skacel, P. Winkel, A. Bilmes, A. V. Ustinov, J. Goupy, M. Calvo, A. Benoit, F. Levy-Bertrand, A. Monfardini, and I. M. Pop, Phys. Rev. Appl. **11**, 054087 (2019).

[22] W. Zhang, K. Kalashnikov, W.-S. Lu, P. Kamenov, T. DiNapoli, and M. E. Gershenson, Phys. Rev. Appl. **11**, 011003 (2019).

[23] P. Kamenov, W.-S. Lu, K. Kalashnikov, T. DiNapoli, M. T. Bell, and M. E. Gershenson, Phys. Rev. Appl. **13**, 054051 (2020).

[24] N. Maleeva, L. Grünhaupt, T. Klein, F. Levy-Bertrand, O. Dupre, M. Calvo, F. Valenti, P. Winkel, F. Friedrich, W. Wernsdorfer, A. V. Ustinov, H. Rotzinger, A. Monfardini, M. V. Fistul, and I. M. Pop, Nat. Commun. **9**, 3889 (2018).

[25] P. Winkel, K. Borisov, L. Grünhaupt, D. Rieger, M. Spiecker, F. Valenti, A. V. Ustinov, W. Wernsdorfer, and I. M. Pop, Phys. Rev. X **10**, 031032 (2020).

[26] L. Grünhaupt, M. Spiecker, D. Gusenkova, N. Maleeva, S. T. Skacel, I. Takmakov, F. Valenti, P. Winkel, H. Rotzinger, W. Wernsdorfer, A. V. Ustinov, and I. M. Pop, Nat. Mater. **18**, 816 (2019).

[27] K. Kalashnikov, W. T. Hsieh, W. Zhang, W.-S. Lu, P. Kamenov, A. D. Paolo, A. Blais, M. E. Gershenson, and M. Bell, arXiv:1910.03769.

[28] T. M. Hazard, A. Gyenis, A. Di Paolo, A. T. Asfaw, S. A. Lyon, A. Blais, and A. A. Houck, Phys. Rev. Lett. **122**, 010504 (2019).

[29] P. Krantz, M. Kjaergaard, F. Yan, T. P. Orlando, S. Gustavsson, and W. D. Oliver, Appl. Phys. Rev. **6**, 021318 (2019).

[30] G. J. Grabovskij, T. Peichl, J. Lisenfeld, G. Weiss, and A. V. Ustinov, Science **338**, 232 (2012).

[31] C. Wang, Y. Y. Gao, I. M. Pop, U. Vool, C. Axline, T. Brecht, R. W. Heeres, L. Frunzio, M. H. Devoret, G. Catelani, L. I. Glazman, and R. J. Schoelkopf, Nat. Commun. **5**, 5836 (2014).

[32] T. Balashov, M. Meyer, and W. Wulfhekel, Rev. Sci. Instrum. **89**, 113707 (2018).

[33] E. R. Pfeiffera and J. F. Schooleya, Phys. Lett. A **29**, 589 (1969).

[34] D. H. Douglass and R. Meservey, Phys. Rev. **135**, A19 (1964).

[35] I.-P. Hong, C. Brun, M. Pivetta, F. Patthey, and W.-D. Schneider, Front. Phys. **1**, 13 (2013).

[36] F. Friedrich, P. Winkel, K. Borisov, H. Seeger, C. Suergers, I. M. Pop, and W. Wernsdorfer, Supercond. Sci. Technol. **32**, 125008 (2019).

[37] D. Sherman, U. S. Pracht, B. Gorshunov, S. Poran, J. Jesudasan, M. Chand, P. Raychaudhuri, M. Swanson, N. Trivedi, A. Auerbach, M. Scheffler, A. Frydman, and M. Dressel, Nat. Phys. **11**, 188 (2015).

[38] S. Nakamura, Y. Iida, Y. Murotani, R. Matsunaga, H. Terai, and R. Shimano, Phys. Rev. Lett. **122**, 257001 (2019).

[39] A. Moshe, N. Bachar, S. Lerer, Y. Lereah, and G. Deutscher, J. Supercond. Nov. Magn. **31**, 733 (2018).

[40] L. Farinacci, G. Ahmadi, G. Reecht, M. Ruby, N. Bogdanoff, O. Peters, B. W. Heinrich, F. von Oppen, and K. J. Franke, Phys. Rev. Lett. **121**, 196803 (2018).

[41] J. C. Cuevas, A. Martín-Rodero, and A. Levy Yeyati, Phys. Rev. B **54**, 7366 (1996).

[42] M. Ternes, W.-D. Schneider, J.-C. Cuevas, C. P. Lutz, C. F. Hirjibehedin, and A. J. Heinrich, Phys. Rev. B **74**, 132501 (2006).

[43] C. Ast, B. Jäck, J. Senkpiel, M. Eltschka, M. Etzkorn, J. Ankerhold, and K. Kern, Nat. Commun. **7**, 13009 (2016).